



HAL
open science

Experimental study and thermodynamic modelling of the Cu-Fe-Si-U sub-systems

L. Soldi, Stéphane Gossé, A. Laplace, P. Bonnaille, J. Schorne-Pinto, M.
Roskosz

► **To cite this version:**

L. Soldi, Stéphane Gossé, A. Laplace, P. Bonnaille, J. Schorne-Pinto, et al.. Experimental study and thermodynamic modelling of the Cu-Fe-Si-U sub-systems. *Journal of Alloys and Compounds*, 2019, 799, pp.239 - 246. 10.1016/j.jallcom.2019.05.294 . hal-03484393

HAL Id: hal-03484393

<https://hal.science/hal-03484393>

Submitted on 20 Dec 2021

HAL is a multi-disciplinary open access archive for the deposit and dissemination of scientific research documents, whether they are published or not. The documents may come from teaching and research institutions in France or abroad, or from public or private research centers.

L'archive ouverte pluridisciplinaire **HAL**, est destinée au dépôt et à la diffusion de documents scientifiques de niveau recherche, publiés ou non, émanant des établissements d'enseignement et de recherche français ou étrangers, des laboratoires publics ou privés.



Distributed under a Creative Commons Attribution - NonCommercial 4.0 International License

Experimental study and thermodynamic modelling of the Cu-Fe-Si-U sub-systems

L. Soldi^{1,*}, S. Gossé¹, A. Laplace², P. Bonnaillie³, J. Schorne-Pinto¹, M. Roskosz⁴

¹ DEN-Service de la Corrosion et du Comportement des Matériaux dans leur Environnement (SCCME), CEA, Université Paris-Saclay, F-91191, Gif-sur-Yvette, France

² DEN-Service d'Etudes de Vitrification et procédés hautes Températures (SEVT), CEA Marcoule, D765, 30200, Chusclan, France

³ DEN-Service de Recherche en Métallurgie Physique (SRMP), CEA, Université Paris-Saclay, F-91191, Gif-sur-Yvette, France

⁴ Muséum National d'Histoire Naturelle, Sorbonne Université, UMR CNRS 7590, Institut de Minéralogie, de Physique des Matériaux et de Cosmochimie, 75005 Paris, France

*Corresponding author: luca.soldi@cea.fr

Abstract

The vitrification is a possible treatment for the conditioning of the metallic Long-Lived Intermediate-Level nuclear waste. This process is characterised by the presence of immiscible oxide and metallic liquids that react each other. A thermodynamic model using the Calphad method is then required to predict the composition of the treated waste and the speciation of uranium in this complex system. The quaternary Cu-Fe-Si-U is chosen as the most representative to describe the metallic liquids that appear at high temperature. Key sub-systems of this quaternary are experimentally investigated and thermodynamically modelled. The description of the *liquidus* in the Si-rich corner of the binary Cu-Si is improved. The Cu-U is assessed with the Calphad method for the first time; it is characterised by a large miscibility gap in the liquid phase. Some new ternary isotherms of the ternary Cu-Fe-Si are then proposed: a large liquid miscibility gap appears also in this system in agreement with the observed behaviour of the metallic liquid during the experimental investigations. The Cu-Si-U system is characterised by three ternary intermetallic compounds: CuSiU, Cu₂Si₂U and Cu₄Si₄U₃. A first description is proposed, but more data are still required to improve the thermodynamic modelling of this system.

Keywords: Calphad; copper; liquid-solid reactions; miscibility gap; phase diagrams; thermodynamic modeling

1. Introduction

The fabrication of Mixed Oxide (MOx) fuel for nuclear power plants is entirely performed in dedicated glove boxes, in order to obtain a homogeneous solid solution of UO₂ and PuO₂ starting from the oxide powders. In the last phase of decommissioning of such glove boxes, all the devices here implemented are contaminated by the presence of actinides (mainly U and Pu) and are therefore classified as Long-Lived Intermediate-Level (LL-IL) nuclear waste. Treatments are required before the definitive disposal of this contaminated waste to avoid any undesirable release of U or Pu in the environment. Vitrification is a possible way for the conditioning of the metallic tools (mainly consisting in stainless steel, copper and aluminium) coming from the glove boxes. The metal waste is melted and mixed with an oxide bath in order to confine U and Pu in a stable glass matrix. In such a complex system, one should expect the formation of two immiscible liquids (an oxide and a metallic) at high temperature. Moreover, the presence of large amounts of Fe and Cu in the metallic reservoir leads to a second phase separation of the metallic liquids into one lighter and rich in Fe and a second one, heavier and rich in Cu. During the vitrification, redox reactions also take place between these three liquids, therefore affecting their chemical compositions. In particular, Al from metallic liquids is oxidised and Si is reduced from the oxide reservoir, reciprocally (Figure 1). Consequently,

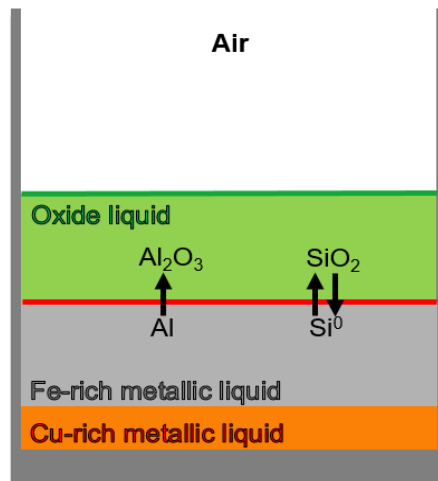


Figure 1 : schematic view of the system appearing at high temperature of the vitrification process for the Long-Lived Intermediate-Level nuclear waste.

the system Cu-Fe-Si-U can be selected as the most representative for the thermodynamic description of the metallic fraction during the entire vitrification process.

In the present work, key sub-systems of the quaternary Cu-Fe-Si-U are studied. Differential Thermal Analysis and Scanning Electron Microscopy with Energy Dispersion Spectroscopy data are implemented to thermodynamically assess the investigated systems thanks to the Calphad approach. In particular, the attention will be focused on the binaries Cu-Si and Cu-U, as well as on the ternaries Cu-Fe-Si and Cu-Si-U.

2. Experimental and Computational Methods

2A: Sample Fabrication

The arc melting technique is well suited to prepare such metallic samples. Ingots of silicon (99.95%_{wt} purity), copper (99.95%_{wt}) and iron (99.9%_{wt}) or uranium (99.965%_{wt}) were weighed in order to obtain a required composition and were placed in a water-cooled copper crucible. Due to the quick oxidation of uranium under ambient conditions, the reactive was immersed in a nitric acid solution and rinsed before melting.

Once the selected elements were placed in the Compact Arc Melter furnace (Edmund Bühler GmbH), the chamber was evacuated to light vacuum conditions and then three times-refilled with high-purity argon (99.9999%_{at}). To assure a better purity of the samples, chunks of an oxygen getter (typically zirconium) were first melted before starting the sample preparations; these operations reduce the oxygen amount in the melting vessel. The arc-melting procedure was repeated three times for each sample to guarantee a good homogenization of the liquid metal. Comparing the masses before and after arc melting resulted in a loss always minor than 1%, considered to be satisfying conditions to ensure a good control of the composition of all the samples.

2B: Differential Thermal Analysis

The Differential Thermal Analysis (DTA) was used to measure the transition temperatures of the analysed samples. Two different thermo-balances were employed during the present study. The first one was a Setaram Setsys 16/18, where all U-free samples were analysed using alumina crucibles. Here, a constant flow of Ar was granted during the entire duration of the tests. The second device was a Mettler TGA/DSC 1 Star System placed in a glove box, for all the measurements involving

samples containing U. In this case, glassy-carbon crucibles and flow of Ar+ 2% H₂ were employed to reduce the oxygen intake by U during the experiments. The DTA data were treated according to the “first detectable departure from baseline” method, as recommended by Boettinger et al. [1]. The experimental procedure for both the devices was very similar: the sample under treatment was heated to the maximum temperature chosen (typically 1500°C for the system Cu-Fe-Si, 1200°C for the ternary Cu-Si-U) at a constant rate. At this point, the temperature was kept constant for 10-20 minutes and then decreased up to 700°C using the same rate as for the last heating performed. This cycle was repeated consecutively three times per sample, adopting rates of 10, 5 and 3°C/min for investigations in the Cu-Fe-Si system, and 20, 10 and 10°C/min for Cu-Si-U. After the third cycle, the sample was cooled to room temperature at the last rate adopted. The first heating and cooling were used as annealing; therefore, the signal here measured was not taken into account to determine any transition temperature, but is reported to show the agreement of the casting samples with the later measurements. The protocol adopted grants to observe samples in equilibrium conditions, required for an accurate and reliable thermodynamic modelling.

2C: Scanning Electron Microscopy and Energy Dispersive Spectroscopy

After the DTA, the samples are polished and observed in a Scanning Electron Microscope (SEM, Zeiss). Both secondary electrons (SE) and backscattered electrons (BSE) modes were used. Phase compositions at equilibrium were evaluated thanks to the Energy Dispersive Spectroscopy (EDS). The energy of the primary beam was chosen between 15 and 20 keV in order to improve the elemental analysis by EDS.

2D: Nano Secondary Ion Mass Spectrometry

The Nano Secondary Ion Mass Spectrometry (NanoSIMS) is an analytical device that performs high-resolution chemical and isotopic analysis in solid samples. The ionic primary beam (with a diameter of 200nm, from an O⁻ source) was focused on the sample and then the secondary ions generated from the collision were collected by an electro-magnetic field and classified depending on their mass-to-charge ratio. Up to five isotopes can be detected at the same moment. This technique was used to analyse some sample belonging to the system Cu-Si-U to obtain an elemental cartography.

2E: Thermodynamic calculations using the Calphad method

The Calphad (CALculation of PHase Diagram) method consists in evaluating the Gibbs free energy for each phase that may appear in a complex chemical system. All the thermodynamic properties can be derived from this energy. Moreover, it is possible to calculate the thermodynamic equilibria of the

Table 1 : Sample Compositions and results for the Cu-Fe-Si ternary

Sample	Composition / % _{at}			Transition temperatures by DTA / °C	Phases by SEM-EDS
	Cu	Fe	Si		
CuFeSi-1	11.8	41.4	46.8	843 / 910 / 1030 / 1077 / 1343	bcc-Fe / fcc-Cu / FeSi
CuFeSi-2	13.6	22.8	63.6	789 / 921 / 1002 / 1158	FeSi ₂ / Diamond-Si / Cu ₃ Si
CuFeSi-3	5.4	87.1	7.5	1085 / 1428 / 1466	bcc-Fe / fcc-Cu
CuFeSi-4	5.3	88.3	6.4	1092 / 1437 / 1474	bcc-Fe / fcc-Cu
CuFeSi-5	14.3	16.6	69.1	800 / 920 / 1064 / 1190	FeSi ₂ / Diamond-Si / Cu ₃ Si
CuFeSi-6	34.1	38.7	27.2	906 / 995 / 1032 / 1109 / 1133	bcc-Fe / fcc-Cu / FeSi
CuFeSi-7	29.0	31.4	39.6	815 / 828 / 1290	FeSi / FeSi ₂ / Cu ₃₃ Si ₇
CuFeSi-8	8.4	53.4	38.2	907 / 1030 / 1100 / 1135 / 1268	bcc-Fe / fcc-Cu / FeSi

Table 2: Sample composition and results for the Cu-Si-U system

Sample	Composition / %at			Transition temperatures by DTA / °C	Phases by SEM-EDS
	Cu	Si	U		
CuSiU-1	42.2	50.8	7.0	800 / 1054	-
CuSiU-2	64.9	10.9	24.2	-	CuSiU / Cu ₅ U / UO ₂
CuSiU-3	64.9	18.4	16.7	956 / 1020 / 1074	fcc-Cu / Cu ₃₃ Si ₇ / Cu ₂ Si ₂ U
CuSiU-4	56.3	29.1	14.6	849 / 904	-
CuSiU-5	61.3	31.6	7.1	800 / 822	-

system by minimising its total Gibbs free energy at given composition, temperature and pressure [2]. Mathematical functions are used to fit the Gibbs energy of the phases from all the experimental data, such as calorimetric measurements, transition temperatures or compositions. In the current work, the Parrot module of the Thermo-Calc software was used to perform the mathematical optimisation [3].

3. Experimental Results

Cu-Fe-Si and Cu-Si-U ternary samples were fabricated using the arc melting technique. Their atomic compositions and all the experimental results obtained during the present research are reported in Table 1 and Table 2 respectively. Herein, the main experimental results concerning the investigated systems are presented.

3A: DTA results

3A.1: Cu-Fe-Si

From the DTA curves of Cu-Fe-Si samples, it appears that the peaks at the highest temperatures are usually wider and are typically attributed to the melting of Fe-rich compounds or to the dissolution of silicon. The formation of Cu-rich liquid occurs at lower temperatures, between 789°C (for sample CuFeSi-2) and 995°C (for sample CuFeSi-6). Minor peaks are due to the formation or dissolution of binary Cu-Si or Fe-Si phases. As an example, the sample CuFeSi-5 DTA curves at different heating rates are shown in Figure 2. Due to the low heat releasing characterising the liquid demixing, no accurate determination of the bimodal curve was achievable with the current technique.

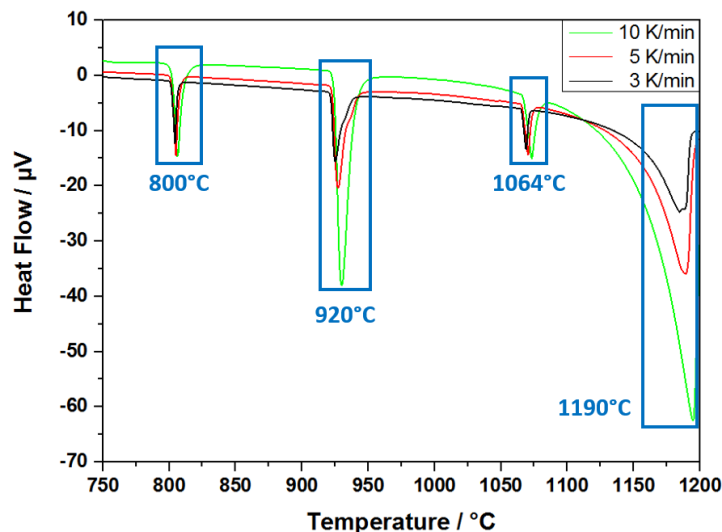


Figure 2 : DTA curves at different heating rates regarding sample CuFeSi-5. The wide peak at 1190°C represents the *liquidus*, while at 800°C formation of liquid Cu is observed.

3A.2: Cu-Si-U

The DTA analyses on Cu-Si-U samples were performed in a reducing environment. Due to the strong embrittlement of the furnace thermocouples caused by the presence of H₂ in the gas flow, the maximum temperature of the experiments were limited to 1200°C and using faster heating rates than for the Cu-Fe-Si system. Therefore, the complete melting could not be granted for all the investigated samples. Nonetheless, these measured transition temperatures measured are still very useful in order to improve the knowledge of the Cu-Si-U.

3B: SEM-EDS and NanoSIMS results

3B.1: Cu-Fe-Si

The EDS analyses of the Cu-Fe-Si system do not reveal any ternary compounds. For example, in sample CuFeSi-8 the only phases formed are those observed in the binaries Cu-Si and Fe-Si, namely bcc-Fe, fcc-Cu and FeSi (Figure 3). The observed microstructure is consistent with the high temperature liquid miscibility gap. First, the Fe-rich liquid solidified in FeSi and bcc-Fe phases, while the Cu-rich one precipitated into fcc-Cu at a lower temperature. The strong separation between Fe-rich and Cu-rich phases highlights the distinct compositions of the liquids from which they formed.

3B.2: Cu-Si-U

The SEM micrographs of sample CuSiU-3 together with the elemental cartography performed using the NanoSIMS analysis are shown in Figure 4. Three phases are identified, namely: fcc-Cu (point 1), totally separated from the two other phases, the ternary compound identified as Cu₂Si₂U (point 2) and a Cu-Si matrix (point 3). From the elemental cartography (Figure 4 right), Cu and Si are found in both the matrix (with a higher signal) and in the intermetallic compound. Uranium (observed in both metallic and oxide states) appears only in the Cu₂Si₂U phase. The strong repulsive interaction between Cu and U can explain the absence of U in the Cu-rich matrix.

The same analysis was performed on the sample CuSiU-2 directly after the arc melting (Figure 5). The SEM micrographs of this sample reveal white euhedral crystals of UO₂ (circle 1), dendrites of the ternary compound CuSiU (point 2) and a Cu-U matrix (point 3). Cu is still found in both the matrix and the intermetallic, Si is almost absent in the matrix and is mainly found in the CuSiU ternary compound. Furthermore, the elemental cartography shows two different behaviours of U (Figure 5 right); the signal of metallic U is stronger in the CuSiU intermetallic compound, while the oxidised UO₂ appears mainly in the matrix.

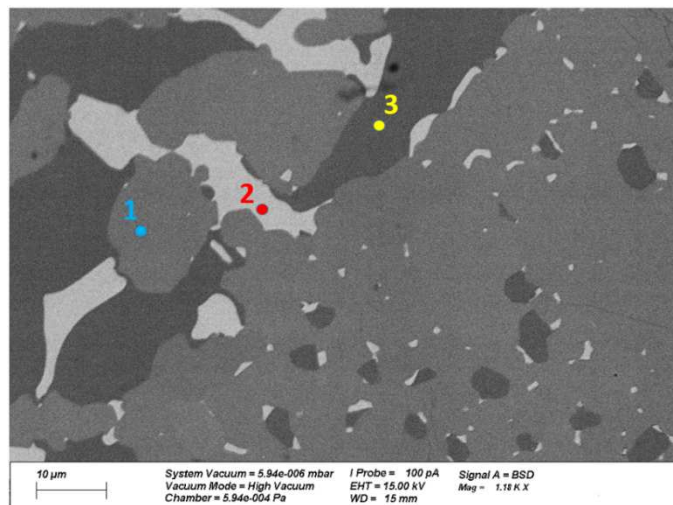


Figure 3 : SEM image of sample CuFeSi-8 obtained in BSE mode. From the EDS analysis, the phases are recognized as: 1) bcc-Fe (1.73%at Cu, 60.09%at Fe and 38.18%at Si); 2) fcc-Cu (89.99%at Cu, 4.37%at Fe and 5.64%at Si); 3) FeSi (2.28%at Cu, 47.85%at Fe and 49.87%at Si). No ternary intermetallic compounds appear here or in other samples of Cu-Fe-Si.

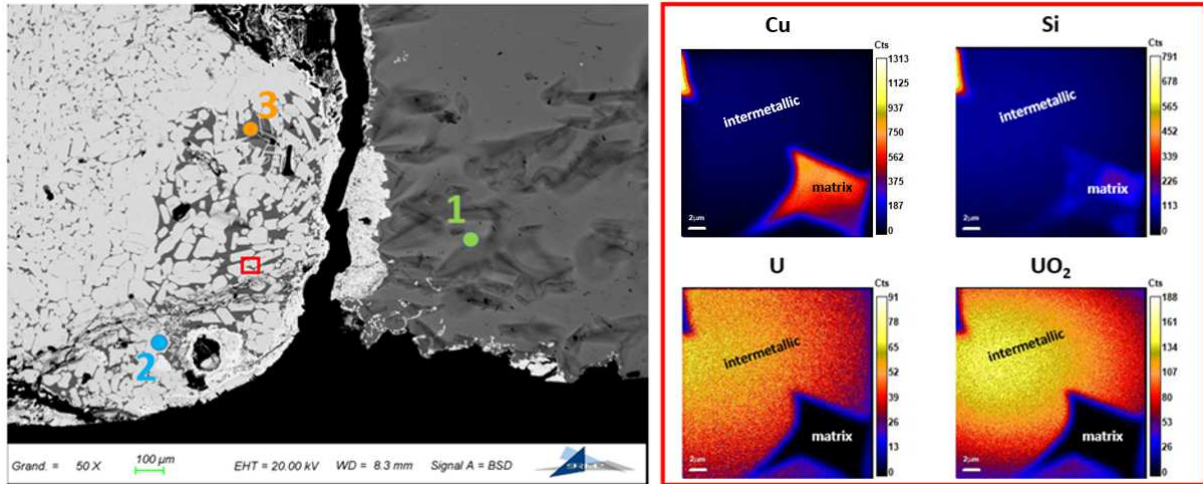


Figure 4 : (left) SEM image of sample CuSiU-3. The phases detected by EDS are: 1) fcc-Cu; 2) $\text{Cu}_2\text{Si}_2\text{U}$ (42.89%_{at} Cu, 31.05%_{at} Si and 21.75%_{at} U, with 4.31%_{at} impurity of O); 3) $\text{Cu}_{33}\text{Si}_7\text{U}$ (82.10%_{at} Cu, 12.72%_{at} Si, 0.03%_{at} U and 5.15%_{at} O). (right) NanoSIMS cartography of the red square reported on SEM image. All U (both in metallic and oxide states) is found in the intermetallic compound.

The sample CuSiU-3 was cooled slowly during DTA and therefore the observed phases are considered to be at equilibrium. This implies that U can solidify and form the intermetallic compound together with Cu and Si. $\text{Cu}_2\text{Si}_2\text{U}$ is the most stable phase for U in these conditions, as confirmed by the low oxygen content measured in this compound. The surrounding Cu-Si matrix results from the solidification of the liquid and only traces of U are found (less than 0.1%_{at}).

On the contrary, quenched sample CuSiU-2 is representative of a high temperature equilibrium, where U is present in both liquid phase and CuSiU compound at the same time. During quenching, all U from the liquid phase cannot solidify into the ternary intermetallic and so remains in the Cu-U matrix. This metallic U is easily oxidised after the experiment, during the storage or during the storage of the samples. This behaviour explains the different location of metallic U and oxidised UO_2 shown by the Nanosims cartography: the former is stabilised by the metallic bond with Cu and Si, capable to prevent the oxidation of uranium; the latter is a consequence of the oxygen interaction with U mixed (without being bonded) with Cu.

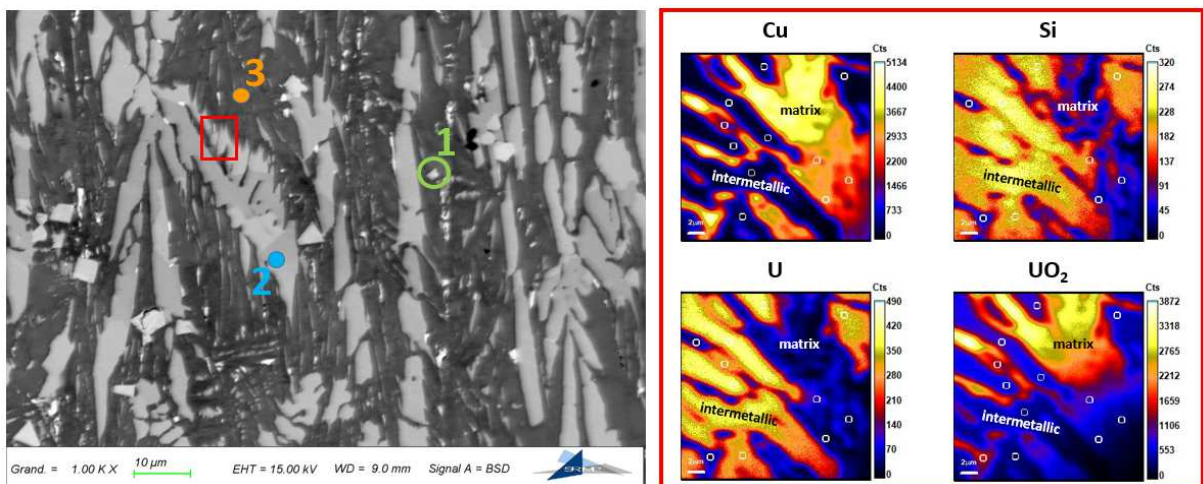


Figure 5 : (left) SEM image of sample CuSiU-2. The phases detected by EDS are: 1) UO_2 (4.39%_{at} Cu, 0.67%_{at} Si, 35.10%_{at} U and 59.84%_{at} O); 2) CuSiU (32.48%_{at} Cu, 28.53%_{at} Si, 31.91%_{at} U and 7.08%_{at} O); 3) Cu_5U (66.36%_{at} Cu, 0.26%_{at} Si and 10.11%_{at} U, with 23.27%_{at} O impurity). (right) NanoSIMS cartography of the red square reported on SEM image. Metallic U is found in the CuSiU phase, while only oxidised U is present in the Cu-U matrix. The bond with Cu and Si stabilises U in its metallic state, while the repulsion interaction with the Cu in the matrix leads to the reaction with the oxygen in the environment.

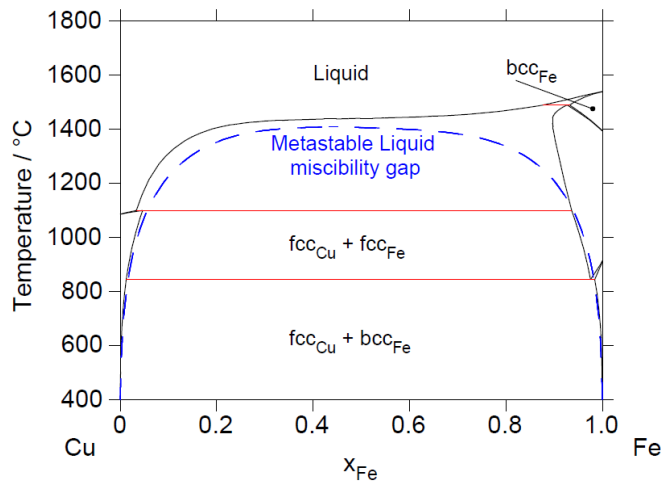


Figure 6 : calculated Cu-Fe phase diagram [4]. The dashed blue line shows the metastable miscibility gap in the liquid phase.

4. Thermodynamic modelling

4A: Binaries from the literature

Six binary systems are required in order to study the quaternary Cu-Fe-Si-U: Cu-Fe, Cu-Si, Cu-U, Fe-Si, Fe-U and Si-U. Four of these binary systems (Cu-Fe [4], Fe-Si [5], Fe-U [6] and Si-U [7]) are taken from the literature; no further investigations were required on these mentioned systems.

Looking at the binary Cu-Fe (Figure 6), it is important to note the presence of miscibility gaps in the fcc phase and a metastable one in the liquid. Such information will be crucial in the latter modelling of the ternary Cu-Fe-Si.

4B: Re-assessment of the Cu-Si binary

Hallstedt et al. [8] proposed recently a new model for the binary Cu-Si. Although the equilibria in the Cu-rich side are well assessed and in good agreement with the available experimental data [9–11], the *liquidus* in the Si-rich part exhibits an unusual shape that may introduce some difficulties in modelling higher order systems. The revised model from Hallstedt et al. [8] proposed here (Figure 7) shows a very good agreement with all the data available in literature. Moreover, the behaviour of the

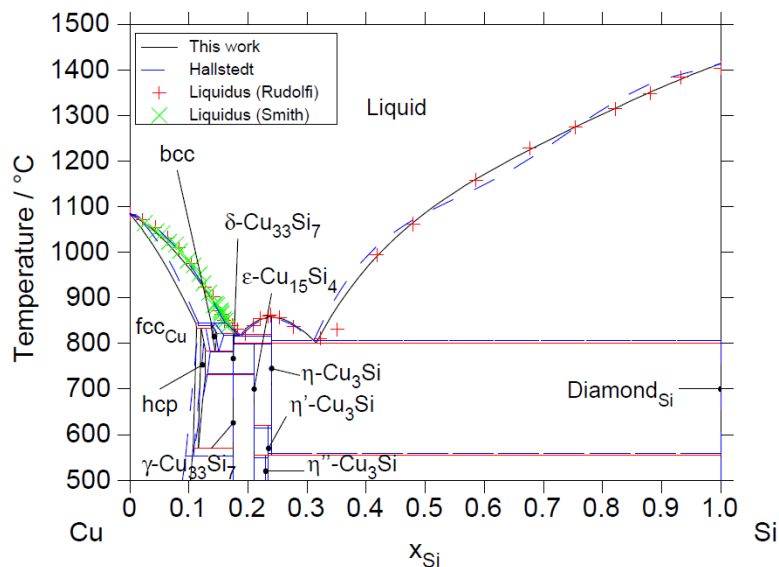


Figure 7 : re-assessed Cu-Si phase diagram compared with experimental data and the previous model of Hallstedt.

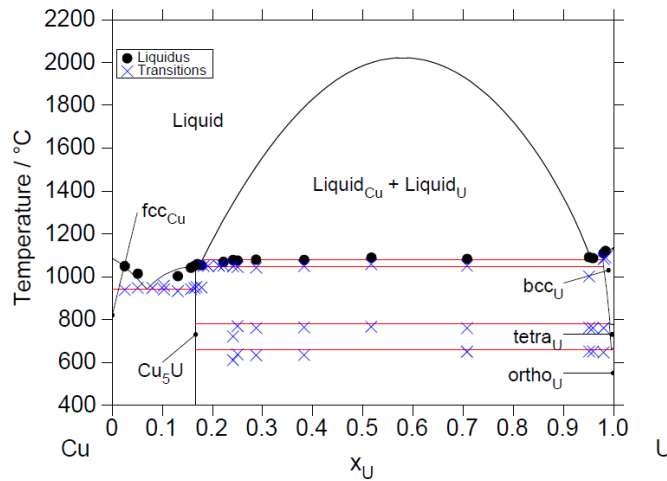


Figure 8 : assessed Cu-U phase diagram with experimental points from Wilhelm and Carson.

liquidus is strongly improved all along the Si-rich corner of the system. This new assessment will be also used for the modelling of higher-order systems involving Cu-Si.

4C: Modelling of the Cu-U system

While several authors have assessed the other binaries, the system Cu-U is the only one lacking of a proper thermodynamic model. To our knowledge, only few studies were dedicated to this system. Rough and Bauer [12] and Massalski et al. [13] reviewed the phase diagram based on the limited experimental dataset available provided by Wilhelm and Carson [14]. One peculiarity of this system is the presence of a large stable miscibility gap in the liquid phase (Figure 8). The optimised thermodynamic parameters are shown in Table 3.

4D: New assessment of the Cu-Fe-Si ternary

The ternary Cu-Fe-Si deserves a special attention because it represents the major ternary in the description of the quaternary Cu-Fe-Si-U due to the mass abundance of these elements in the quaternary system. Although thermodynamic descriptions of the ternary Cu-Fe-Si exist in literature, the improved version of the binary Cu-Si imposed a dedicated assessment for this ternary, taking into account the experimental data described above and the dataset available from the literature [15–19].

The derived model is in very good agreement with all the datasets used during the optimisation. For example, Figure 9 shows the isothermal section at 1000°C as compared to the results of Wang et al. [18] and the section at 1400°C, where a large liquid miscibility gap appears.

In Figure 10, the thermodynamic model is then used to calculate the solidification path at a typical mean amount of metallic contaminated waste (15%_{wt} Cu, 80%_{wt} Fe and 5%_{wt} Si). It can be useful also

Table 3 : Thermodynamic parameters for the Cu-U binary

Phase	Sublattice model	Thermodynamic Parameters [J/mol]
Liquid	(Cu,U) ₁	${}^0L_{Cu,U}^{liq} = 74118 - 30.51 * T$ ${}^1L_{Cu,U}^{liq} = -23863 + 0.58 * T$ ${}^2L_{Cu,U}^{liq} = -28744$
Bcc	(Cu,U) ₁ , Va ₁	${}^0L_{Cu,U}^{bcc} = 37540$
Fcc	(Cu,U) ₁ , Va ₁	${}^0L_{Cu,U}^{fcc} = 16192$
Orthorhombic	(Cu,U) ₁	${}^0L_{Cu,U}^{ortho} = 129564$
Tetragonal	(Cu,U) ₁	${}^0L_{Cu,U}^{tetra} = 34061$
Cu ₅ U	Cu ₅ , U ₁	${}^0G_{Cu:U}^{Cu5U} = GHSERU + 5 * GHSERCU + 5761 - 22.84 * T$

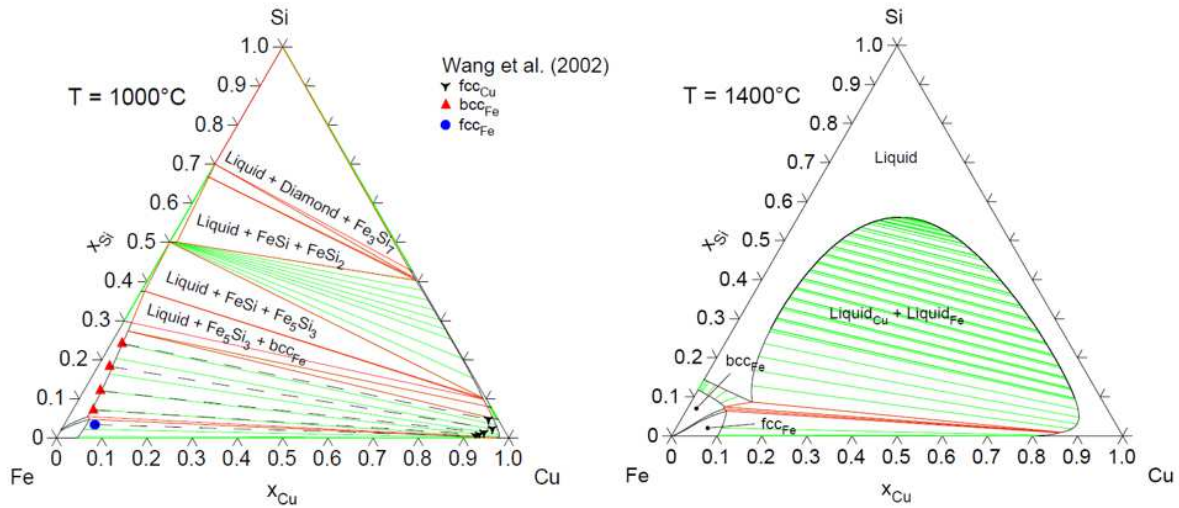


Figure 9 : isothermal sections at 1000°C (left) and 1400°C (right). On the left, the experimental data from Wang are compared with the calculations. On the right, a large miscibility gap in the liquid appears clearly.

considering the domestic waste incineration residue, as reported by Hino et al. [17]. From the calculations, the liquid miscibility gap appears in the short temperature range between 1396 (*liquidus*) and 1374°C. In the miscibility gap, the Cu-rich liquid contains about 90%_{at} Cu, while the Fe-rich about 77%_{at} Fe. At 1374°C, the Cu-rich liquid is in equilibrium with bcc-Fe until the temperature of 1090°C, when it solidifies in fcc-Cu.

4E: First assessment of Cu-Si-U

In the framework of the vitrification of LL-IL nuclear waste, another pivotal system to study is the ternary Cu-Si-U. No previous thermodynamic assessments were found for this system. The only information concerning ternary phases focuses on low temperature magnetic properties of Cu-Si-U intermetallic compounds [20–27]. From these studies, three ternary intermetallic compounds have been identified: CuSiU, Cu₂Si₂U and Cu₄Si₄U₃. The ternary phase CuSiU is modelled considering the partial substitution of Cu in the Si sublattice of the phase USi_{1.88}, as pointed out by Pöttgen and Kaczorowski [23]. Pechev et al. [20] highlighted a change in the crystallographic structure of such intermetallic compound, depending on the content of Cu (tetragonal α -ThSi₂ prototype for low content of Cu, hexagonal AlB₂ for higher content); in the current modelling only the structure type α -ThSi₂ is considered. The Cu₂Si₂U compound has a tetragonal structure and a stoichiometric composition [26], while the Cu₄Si₄U₃ is characterised by an orthorhombic structure and a non-

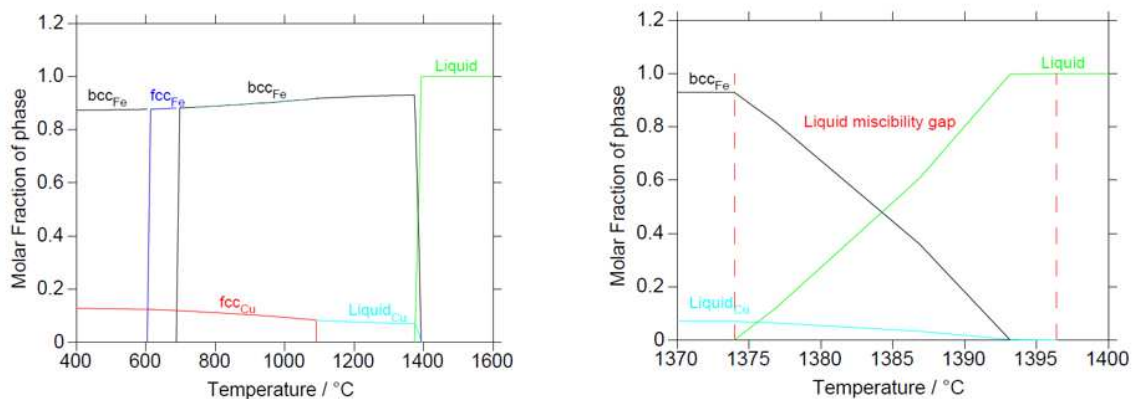


Figure 10 : solidification pathways at the composition 15%_{wt} Cu, 80%_{wt} Fe and 5%_{wt} Si between 400 and 1600°C (left) and a zoom between 1370 and 1400°C (right) to highlight the presence of the liquid miscibility gap.

Table 4: crystallographic data on ternary compounds of Cu-Si-U

Phase	Prototype	Lattice parameters [nm]			Reference
		<i>a</i>	<i>b</i>	<i>c</i>	
CuSiU	α -ThSi ₂	0.3979	-	1.3929	[20]
Cu₂Si₂U	ThCr ₂ Si ₂	0.398	-	0.995	[21]
Cu₄Si₄U₃	Ni ₄ Si ₄ U ₃	0.3963	0.4022	2.3836	[22]

stoichiometric behaviour (low excess of Si relative to Cu [22]). The lattice parameters of these compounds are reported in Table 4.

Very useful information is obtained from the experimental DTA results discussed previously. The available data on the three ternary compounds have been added to the model to thermodynamically assess the Cu-Si-U (Figure 11). Still, they do not provide enough understanding to derive a satisfying description. In particular, more data are still needed to define precisely their composition and temperature ranges of existence. However, the current model shows a lower extent of the liquid miscibility gap (as expected from the Cu-U binary) when compared to the Cu-Fe-Si ternary miscibility gap. This result is partly due to the formation of ternary intermetallic compounds.

5. Conclusions

In the framework of the study on the vitrification process for the metallic LL-IL nuclear waste, crucial sub-systems of the quaternary Cu-Fe-Si-U have been investigated experimentally and then thermodynamically assessed using the Calphad method. The binary Cu-Si has been re-assessed starting from the model of Hallstedt et al. [8] keeping the good modelling in the Cu-rich side and improving the *liquidus* of the Si-rich side. The first thermodynamic assessment of Cu-U is performed using the few data available in literature [14]. From these binaries, the attention has been focused on crucial ternary systems. Cu-Fe-Si is characterised by a large miscibility gap in the liquid phase and no ternary compounds have been found; the thermodynamic model is in good agreement with all the data coming from the literature. Cu-Si-U is thermodynamically assessed for the first time; in such a system, three ternary intermetallic compounds are considered in the model. However, more experimental results are still needed in order to have a better description, especially regarding the temperature and composition ranges of existence for each of the ternary intermetallic compounds.

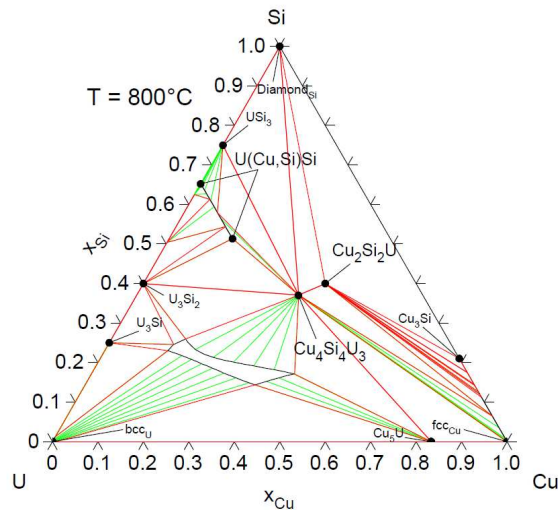


Figure 11 : isothermal section at 800°C of the Cu-Si-U ternary; the three intermetallic compounds are highlighted.

Acknowledgements

This work was funded by the Direction of Nuclear Energy of CEA. The authors would like to thank C. Bonnet (CEA, LM2T) for carrying out part of the experiments. A special acknowledgement is dedicated to R. Duhamel and S. Mostefaoui (National Museum of Natural History) for the help provided during the analyses with the NanoSIMS.

References:

- [1] W.J. Boettinger, U.R. Kattner, J.H. Perepezko, DTA and Heat-flux DSC Measurements of Alloy Melting and Freezing, (n.d.) 100.
- [2] H.L. Lukas, S.G. Fries, B. Sundman, Computational thermodynamics: the CALPHAD method, Cambridge University Press, Cambridge ; New York, 2007.
- [3] B. Sundman, B. Jansson, J.-O. Andersson, The Thermo-calc databank system, Calphad. 9 (1985) 153–190.
- [4] I. Ansara, Europäische Gemeinschaften, eds., Definition of thermochemical and thermophysical properties to provide a database for the development of new light alloys:: COST 507. Vol. 2: Thermochemical database for light metal alloys, Off. for Off. Publ. of the Europ. Communities, Luxembourg, 1998.
- [5] J. Lacaze, B. Sundman, An assessment of the Fe-C-Si system, MTA. 22 (1991) 2211–2223. doi:10.1007/BF02664987.
- [6] M. Kurata, Thermodynamic database on U-Pu-Zr-Np-Am-Fe alloy system II — Evaluation of Np, Am, and Fe containing systems-, IOP Conference Series: Materials Science and Engineering. 9 (2010) 012023. doi:10.1088/1757-899X/9/1/012023.
- [7] A. Berche, C. Rado, O. Rapaud, C. Guéneau, J. Rogez, Thermodynamic study of the U–Si system, Journal of Nuclear Materials. 389 (2009) 101–107. doi:10.1016/j.jnucmat.2009.01.014.
- [8] B. Hallstedt, J. Gröbner, M. Hampl, R. Schmid-Fetzer, Calorimetric measurements and assessment of the binary Cu–Si and ternary Al–Cu–Si phase diagrams, Calphad. 53 (2016) 25–38. doi:10.1016/j.calphad.2016.03.002.
- [9] E. Rudolphi, Metallographische Mitteilungen aus dem Institut für anorganische Chemie der Universität Göttingen. XLIII. Die Silicide des Kupfers, Z. Anorg. Chem. 53 (1907) 216–227. doi:10.1002/zaac.19070530115.
- [10] Smith, The alpha-based boundary of the copper-silicon system, Journal of the Institute of Metals. 40 (1928) 359–373.
- [11] K. Sufryd, N. Ponweiser, P. Riani, K.W. Richter, G. Cacciamani, Experimental investigation of the Cu–Si phase diagram at $x(\text{Cu}) > 0.72$, Intermetallics. 19 (2011) 1479–1488. doi:10.1016/j.intermet.2011.05.017.
- [12] F.A. Rough, A.A. Bauer, Constitution of uranium and thorium alloys, Metallurgy and Ceramics, 1958.
- [13] T.B. Massalski, H. Okamoto, P.R. Subramanian, L. Kacprzak, Binary alloy phase diagrams, Second edition, Second, The Materials Information Society, 1990.
- [14] H.A. Wilhelm, O.N. Carlson, The uranium-manganese and uranium-copper alloy systems, Trans. Am. Soc. Metals. (1950) 1311.
- [15] J. Zhao, L. Zhang, Y. Du, H. Xu, J. Liang, B. Huang, Experimental Investigation and Thermodynamic Reassessment of the Cu-Fe-Si System, Metall and Mat Trans A. 40 (2009) 1811–1825. doi:10.1007/s11661-009-9877-2.
- [16] X. Li, Z. Li, Experimental Investigation of the 650 °C Isothermal Section of the Cu-Fe-Si Ternary Phase Diagram, Journal of Phase Equilibria and Diffusion. (2017). doi:10.1007/s11669-017-0519-x.
- [17] M. Hino, T. Nagasaka, T. Washizu, Phase diagram of Fe-Cu-Si ternary system above 1523 K, JPE. 20 (1999) 179. doi:10.1361/105497199770335695.

- [18] C.P. Wang, X.J. Liu, I. Ohnuma, R. Kainuma, K. Ishida, Phase equilibria in Fe-Cu-X (X: Co, Cr, Si, V) ternary systems, *JPE*. 23 (2002) 236. doi:10.1361/105497102770331712.
- [19] H. Ohtani, H. Suda, K. Ishida, Solid/Liquid equilibria in Fe-Cu based ternary systems, *ISIJ International*. 37 (1997) 207–216.
- [20] S. Pechev, B. Chevalier, B. Darriet, J. Etourneau, Structural chemistry and magnetic behaviour of the ternary silicides UCu_xSi_{2-x} ($0.28 \leq x \leq 0.96$), *Journal of Alloys and Compounds*. 282 (1999) 44–51. doi:10.1016/S0925-8388(98)00817-2.
- [21] M.W. McElfresh, L. Rebelsky, M.S. Torikachvili, H. Borges, K. Reilly, S. Horn, M.B. Maple, Magnetic phase diagrams of UCu_2Si_2 and UNi_2Si_2 , *Journal of Applied Physics*. 67 (1990) 5218–5220. doi:10.1063/1.344615.
- [22] S. Pechev, B. Chevalier, D. Laffargue, B. Darriet, T. Roisnel, J. Etourneau, Magnetic behavior of the ternary silicide $U_3Cu_4Si_4$, *Journal of Magnetism and Magnetic Materials*. 191 (1999) 282–290. doi:10.1016/S0304-8853(98)00358-8.
- [23] R. Pöttgen, D. Kaczorowski, Synthesis and characterization of some new ternary uranium transition metal silicides U_2TSi_3 ($T \equiv Fe, Co, Ni, Cu, Ru, Rh, Pd, Os, Ir, Pt, Au$) with disordered AlB_2 - and α - $ThSi_2$ -type structures, *Journal of Alloys and Compounds*. 201 (1993) 157–159. doi:10.1016/0925-8388(93)90877-P.
- [24] J. Leciejewicz, A. Szytuła, P. Rogl, Magnetic structure of $U_{0.5}Y_{0.5}Cu_2Si_2$, *Journal of Magnetism and Magnetic Materials*. 119 (1993) 167–170. doi:10.1016/0304-8853(93)90517-6.
- [25] D. Kaczorowski, H. Noël, M. Potel, Structural, magnetic and electrical properties of new uranium intermetallics: $U_3Cu_4Si_4$ and $U_3Cu_4Ge_4$, *Physica B: Condensed Matter*. 206 (1995) 457–460. doi:10.1016/0921-4526(94)00489-I.
- [26] K. Hiebl, P. Rogl, C. Horvath, K. Remschnig, H. Noël, Magnetism and structural chemistry of $U_{1-x}Y_xCu_{2+y}Si_{2-y}$, $U_{1-x}Y_xCr_2Si_2$, and $U(Cu_{1-x}Cr_x)_2Si_2$ alloys, *Journal of Applied Physics*. 67 (1990) 943–948. doi:10.1063/1.345729.
- [27] T. D. Matsuda, Y. Haga, S. Ikeda, A. Galatanu, E. Yamamoto, H. Shishido, M. Yamada, J.-I. Yamaura, M. Hedo, Y. Uwatoko, T. Matsumoto, T. Tada, S. Noguchi, T. Sugimoto, K. Kuwahara, K. Iwasa, M. Kohgi, R. Settai, Y. Ōnuki, Electrical and Magnetic Properties of a Single Crystal UCu_2Si_2 , *Journal of the Physical Society of Japan*. 74 (2005) 1552–1556. doi:10.1143/JPSJ.74.1552.